ADVANCED THEORY AND SIMULATIONS
www.advtheorysimul.com

Quantum Nuclei at Weakly Bonded Interfaces: The Case of Cyclohexane on Rh(111)

Karen Fidanyan, Ikutaro Hamada, and Mariana Rossi**

The electronic properties of interfaces can depend on their isotopic constitution. One known case is that of cyclohexane physisorbed on Rh(111), in which isotope effects have been measured on the work function change and desorption energies. These effects can only be captured by calculations including nuclear quantum effects (NQE). In this paper, this interface is addressed employing dispersion-inclusive density-functional theory coupled to a quasi-harmonic (QH) approximation for NQE, as well as to fully anharmonic ab initio path integral molecular dynamics (PIMD). The QH approximation is able to capture that deuterated cyclohexane has a smaller adsorption energy and lies about 0.01 Å farther from the Rh(111) surface than its isotopologue, which can be correlated to the isotope effect in the work function change. An investigation of the validity of the QH approximation relying on PIMD simulations, leads to the conclusion that although this interface is highly impacted by anharmonic quantum fluctuations in the molecular layer and at bonding sites, these anharmonic contributions play a minor role when analyzing isotope effects at low temperatures. Nevertheless, anharmonic quantum fluctuations cause an increase in the distance between the molecular layer and Rh(111), a consequent smaller overall work function change, and intricate changes in orbital hybridization.

1. Introduction

Usually, the electronic properties of interfaces do not strongly depend on the isotopic constitution of the atoms that compose them. This is because the electronic structure of different isotopes is the same and nuclei can typically be considered as classical particles, which means that an isotopic change cannot lead to a change in the (static) atomic structural properties of materials, and thus do not cause a change in the electronic structure. However, when the quantum nature of the nuclei makes itself more prominent, this ceases to be true. An isotopic change can lead to structural changes of the material and thus to a considerable change in the electronic structure. Such electron-phonon coupling effects can be captured to a great extent in the adiabatic limit.[1] In this case, electronic properties can be modified because of their dependence on the nuclear positions and the equilibrium nuclear fluctuations at any given temperature.

One known case to exhibit such isotopic effects is cyclohexane (C_6H_{12}) adsorbed on platinum-group metal surfaces. It was shown in a series of papers by Koitaya, Yoshinobu, and coworkers,[2,3] that the change of work function induced by adsorbed cyclohexane is different when considering C_6H_{12} and fully deuterated C_6D_{12}. Based on work function measurements and previous calculation of alkanes on metal surfaces,[4] it was suggested that deuterated molecules should lie farther from the surface. Also the desorption energy differs significantly: that of C_6H_{12} on Rh(111) is 84 ± 23 meV higher than that of C_6D_{12} at lower coverages, thus showing an inverse kinetic isotope effect. In these systems, such effects are of a certain relevance because changes in the strength of the bond between hydrogen and metal and between hydrogen and carbon impact the dehydrogenation propensity of cyclohexane—a molecule that often plays a central role in systems aiming at cheap high-density hydrogen storage.[5] The availability of experimental data and the importance of these systems thus make them an ideal ground to study the performance of different theoretical techniques in a complex but well-defined environment.

The challenges for theory to tackle this problem stem from the necessity of capturing complex electronic-structure changes, as well as the multidimensional atomic structure of quantum nuclei. In particular, electron–phonon coupling needs to be included at least in an approximate fashion in order to relate

K. Fidanyan, M. Rossi
Fritz Haber Institute of the Max Planck Society
Faradayweg 4-6, Berlin 14195, Germany
E-mail: mariana.rossi@mpsd.mpg.de
K. Fidanyan, M. Rossi
Max Planck Institute for the Structure and Dynamics of Matter
Luruper Chaussee 149, Hamburg 22761, Germany
I. Hamada
Department of Precision Engineering
Graduate School of Engineering
Osaka University
2-1 Yamadaoka Suita, Osaka 565-0871, Japan
E-mail: ihamada@prec.eng.osaka-u.ac.jp

The ORCID identification number(s) for the author(s) of this article can be found under https://doi.org/10.1002/adts.202000241

DOI: 10.1002/adts.202000241

nuclear fluctuations and electronic-structure variations. Modeling these effects becomes more important as the field moves toward soft and hybrid electronic materials, where electron–phonon coupling tends to be more pronounced.[6,7] A common way to address such problems is to employ the harmonic approximation for the nuclear vibrations on first-principles potential energy surfaces.[8] However, the validity of this approximation in weakly bonded systems and interfaces, where anharmonic terms in the potential energy surface are expected to play a role, is questionable.

Instead, a method capable of including NQE without relying on the harmonic approximation is ab initio path integral molecular dynamics (aiPIMD).[9] Despite its immense potential, a significant drawback of aiPIMD simulations is their high computational cost. Therefore, in this work, aiPIMD simulations are performed making use of a technique that reduces the amount of replicas required for simulations of weakly-bonded interfaces.[10] These results are compared to harmonic and quasi-harmonic approximations. With these simulations, we are able to explain the physical origin of the observed isotope effects on the cyclohexane/Rh(111) interface and identify when a quasi-harmonic analysis of these effects is valid. We study the impact of nuclear quantum fluctuations on the electronic structure taking advantage of the aiPIMD simulations—an approach that has been successfully applied previously on diverse systems.[11–13] The capabilities and limitations of aiPIMD based on density-functional theory (DFT) are further discussed for this system.

2. Results and Discussion

Experimental measurements conducted on the cyclohexane/Rh(111) interface have shown that several aspects of the adsorption show a dependence on the coverage.[2] In particular, desorption competes with dehydrogenation at coverage values below 0.5. We therefore built models for the different coverages, based on existing experimental data. On a clean Rh(111) surface, experiment shows a high-order large commensurate $(2\sqrt{79}\times 2\sqrt{79})R17.0°$ pattern.[14] This system size would not be computationally tractable, given the amount of ab initio simulations necessary to investigate nuclear quantum effects in this system. A smaller commensurate structure that was also observed in experiment is a $(2\sqrt{3}\times 2\sqrt{3})R13.9°$ pattern,[15] shown in **Figure 1**a. This structure was taken as a reference for the full-coverage monolayer structure. The effective coverage for other structures derived from this one were calculated, and smaller unit cells for lower coverage were modelled. These models are shown in Figure 1b–d. In the following, we perform our calculations principally on the structure presented in Figure 1c ($\theta = 0.46$) unless explicitly stated otherwise. This supercell, containing two cyclohexane molecules and a Rh(111) (5×5) surface cell, allows us to partially capture the phonon band structure dispersion, which is especially pronounced for the metal surface,[16] in the real-space dynamics simulations.

2.1. Static Results and the Quasi-Harmonic Approximation

For the different coverages shown in Figure 1, the adsorption energy $E_{\mathrm{ads}}^{\mathrm{pot}}$ per molecule was calculated as explained in Experimental Section. The results employing the PBE+vdW$^{\mathrm{surf}}$[17,18] functional are reported in column 2 of **Figure 2**a.

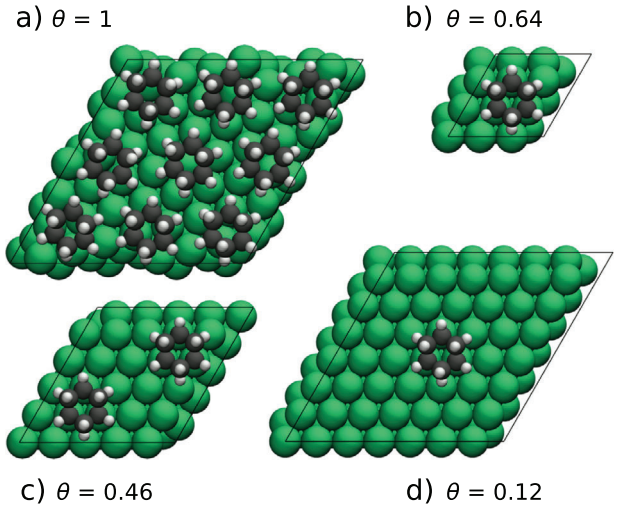

Figure 1. The cyclohexane adsorption patterns considered in this work for modeling different coverages θ. a) $\theta = 1$, $(2\sqrt{3}\times 2\sqrt{3})R13.9°$ unit cell (0.173 molecules per Rh atom). b) $\theta = 0.64$, (3×3) unit cell. c) $\theta = 0.46$, (5×5) unit cell. d) Coverage $\theta = 0.12$, (7×7) unit cell.

The harmonic free energy terms at a temperature of 150 K was added to the adsorption energy, as given by Equation (6). This temperature was chosen to satisfy several conditions. On one hand, the temperature should be below the temperature of desorption and dehydrogenation, which are both close to 200 K.[2] On the other hand, very low temperatures considerably increase the cost of a PIMD simulation and would reduce the role of anharmonicity, which we aim to investigate. The adsorption free energies $F_{\mathrm{ads}}^{\mathrm{harm}}$ were obtained analogously to Equation (5).

The results for each coverage are summarized in Figure 2a, columns 3–8. The addition of the zero point energy and the temperature-dependent free energy terms, already in the harmonic approximation, lead to a different adsorption energy for C_6H_{12} and C_6D_{12}. This is to be expected because the C-H stretching modes of the adsorbed cyclohexane associated with the CH groups that point to the surface show a significant red shift of up to 300 cm^{-1} in comparison to the gas phase, as shown in Figure S2, Supporting Information. Because of the difference in mass between the H and D atoms, such a red shift has a stronger impact on the ZPE of a C-H vibration, compared to a C-D one, as schematically shown in Figure 2b. In both cases, the effect of ZPE increases the energy of adsorption (Figure 2a, columns 3,4), and in the case of C_6H_{12}, this effect is stronger. When adding the full free energy contributions, the translational and rotational entropic contributions of the gas-phase molecules work to decrease the adsorption free energy (Figure 2a, columns 6,7). The magnitude of the isotope effect is not strongly affected by temperature and is about a factor two smaller than what is observed in temperature-programmed desorption experiments,[2] as shown in Figure 2a. We also observe that the difference between H/D adsorption energies becomes smaller at full coverage. It decreases from 37 meV for $\theta = 0.12$ to 20 meV for $\theta = 1$. This trend appears because the red shift of surface-pointing C-H stretch modes decreases with increasing coverage, implying a weaker

a)

coverage θ	E_{ads}^{pot}	E_{ads}^{pot}+ZPE(H)	E_{ads}^{pot}+ZPE(D)	Δ ZPE	F_{ads}^{harm}(H)	F_{ads}^{harm}(D)	ΔF(H – D)
0.12	945	1039	1004	35	742	705	37
0.46	953	1056	1022	34	786	750	36
0.64	946	1046	1013	33	780	745	35
1.0	1023	1066	1049	17	790	770	20
0.3 (TPD [2])		728 ± 12	644 ± 20	84 ± 23			

b)

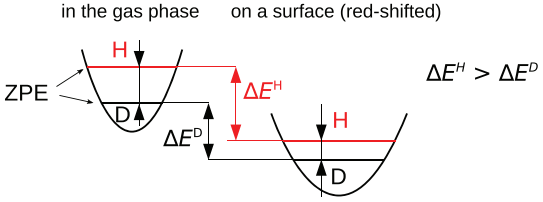

Figure 2. a) Adsorption energies and harmonic free energies for different coverage values, calculated with the PBE+vdW^{surf} functional (*light* settings) according to Equation (5). The free energy is calculated for the temperature of 150 K and all energies are in meV. Experimental data from temperature programmed desorption (TPD) experiments from ref. [2]. Comparison between *light* and *tight* computational settings for these quantities is shown in Table S1, Supporting Information. b) The effect of the red shift in the C-H stretching modes on the adsorption energy, shown schematically. The difference in ZPE is between H and D is higher in vacuum than on surface, due to the different masses and the red-shift of the corresponding stretching mode upon binding.

molecule-surface interaction (Figure S2, Supporting Information). This confirms the weakening of the Rh-H bond with increasing coverage (and consequent strengthening of the C-H bond).

In order to investigate the impact of the exchange-correlation functional on the description of this system, we have computed the adsorption profiles of cyclohexane on Rh(111) with different functionals and vdW corrections. In **Figure 3**a, we show the adsorption curve with the PBE functional, the PBE+vdW^{surf} functional, the PBE functional with the recently proposed many-body dispersion method nl-MBD,[19] the range-separated hybrid functional HSE06[20] combined with nl-MBD dispersion interactions, and the non-local rev-vdW-DF2[21] functional (see Experimental Section for the details of calculations), all for the coverage of $\theta = 0.46$. The minima of these curves are tabulated in Table S2, Supporting Information. The rev-vdW-DF2 calculation was performed only at the equilibrium position and at the reference geometries (i.e., isolated slab and molecule). Further calculations of the binding curve with this functional for a different coverage ($\theta = 0.64$) are reported in Section S3 and Table S3, Supporting Information.

We start by analyzing the dataset based on the PBE functional, which allows us to understand the impact of different descriptions of the vdW corrections. Comparing the result obtained with the bare PBE functional and the others, we conclude, as expected, that vdW interactions are a fundamental piece of the molecule-surface interaction. We then proceed to compare the results obtained with PBE+vdW^{surf} with the results obtained with PBE+nl-MBD. Both of these vdW corrections do not enter the Kohn–Sham potential within the self-consistent procedure, such that they cannot change the electronic density. We observe that vdW^{surf} predicts a larger binding energy (0.90 eV) and an equilibrium distance closer to the surface (3.36 Å) than nl-MBD (0.84 eV and 3.45 Å, respectively). Considering that nl-MBD contains explicit many-body vdW effects and captures the electronic screening of these interactions better than vdW^{surf},[19] we can conclude that the observed differences are due to both of these effects. Then, we can compare the results obtained with the PBE+nl-MBD and the HSE06+nl-MBD functionals. In this case, the vdW interactions are treated at the same level, but the short-range exchange term is modified to include a fraction of exact exchange. The changes in the electronic density brought by the HSE06 functional produce a larger binding energy (1.03 eV) and an equilibrium position that is even closer to the surface (3.30 Å). These observations, combined, point to the prediction of stronger bonds between surface and adsorbate when the self-interaction error is mitigated. Finally, the rev-vdW-DF2 functional, which improves the description of the polarizability of these systems, predicts the adsorption distance of 3.48 Å and binding energy of 0.77 eV, which is smaller than those obtained with other functionals. The experimental values from TPD experiments lie closer to the PBE+nl-MBD and rev-vdW-DF2 binding energies. The shape of the potential along the desorption coordinate hints that anharmonic effects on this coordinate or others that couple with it could have an important effect on the adsorption properties of this system, and potentially on nuclear quantum effects. For further investigation, we employ *light* settings of the FHI-aims code and a comparison of the adsorption curve computed with *tight* and *light* settings is shown in Figure S1, Supporting Information.

In order to investigate the impact of nuclear quantum effects including anharmonicity at least on the desorption coordinate, harmonic phonons and the corresponding zero-point-energy contribution to the adsorption energy for the adsorbed $C_6H(D)_{12}$ at different distances to Rh surface were calculated. At each desired distance, we have fixed the center of mass of the molecule, and optimized the other degrees of freedom except the two bottom layers. See the discussion in the Section S4, Supporting Information, regarding the inclusion of different vibrational modes in this ZPE correction. The quasi-harmonic (QH) ZPE-corrected energy of adsorption E_{ads}^{*} was then calculated according to Equation (7). These values were calculated with the PBE+vdW^{surf} functional, because it delivers a good description of the desorption curve, and its computational cost and implementation in the FHI-aims code allow a fast computation of thousands

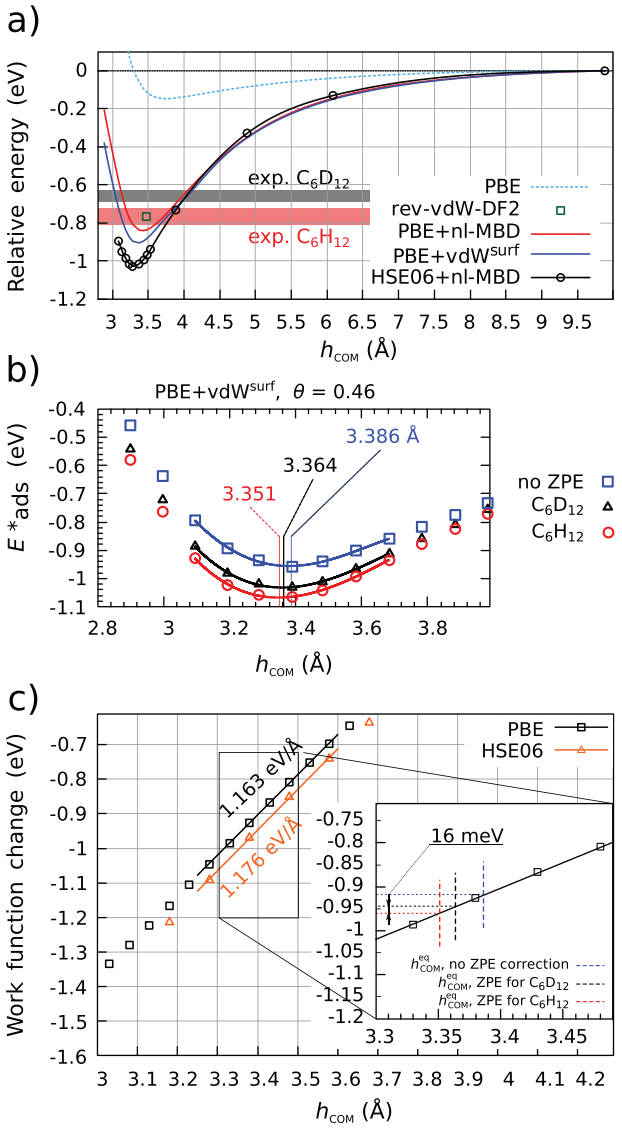

Figure 3. a) Adsorption curves calculated with different exchange-correlation functionals and vdW corrections: PBE (dotted blue line), PBE +vdW^{surf} (solid blue line), PBE+nl-MBD (solid red line), HSE06+nl-MBD (black points), and rev-vdW-DF2 (green square, equilibrium distance only). Calculations were performed with the unit cell of $\theta = 0.46$. Shaded areas show the interval of reported experimental values of the adsorption energy of C_6H_{12} (red) and C_6D_{12} (grey) around the coverages we study.[2] b) ZPE-corrected energy of adsorption for C_6H_{12} (red) and C_6D_{12} (black), calculated according to Equation (7) with PBE + vdW^{surf}. Blue line shows the adsorption energy values calculated without ZPE correction. c) Work function change as a function of distance to surface, calculated with PBE (black squares) and HSE06 (orange triangles). Vertical dashed lines in the inset mark the equilibrium distances for classical nuclei (blue), C_6D_{12} (black), and C_6H_{12} (red).

of force evaluations—which is not the case for the other functionals we show here. The results are presented in Figure 3b. The adsorption energies and distances obtained for C_6H_{12} and C_6D_{12} in this way are also summarized in Table S5, Supporting Information. With this procedure, a deformation of the binding energy curve that is different for C_6H_{12} and C_6D_{12} is predicted, such that C_6H_{12} has a larger binding energy and adsorbs closer to the surface than C_6D_{12}. The H-D adsorption energy difference is 37 meV for PBE + vdW^{surf} functional, which is slightly larger than the value reported in Figure 2a. In Figure S3, Supporting Information, we show a comparison of this QH procedure with the rev-vdW-DF2 functional and a different coverage, which confirms that the effect of ZPE on these curves is quite similar across different coverages and functionals. We have checked that adding finite temperature contributions in the harmonic approximation to these values, up to 150 K, also does not appreciably change this calculated isotope effect (see Figure S4, Supporting Information).

Regarding the equilibrium distance of absorption, there is an important effect that is observed. The adsorption distance of C_6H_{12} is 3.351 Å, and for C_6D_{12}, it is 3.364 Å. The H-D equilibrium distance difference is thus ≈0.01 Å. Although apparently small, this equilibrium distance difference has a marked effect on the work function changes. The sensitivity of the work function change $\Delta\phi$ of the interface to the distance between the adsorbate and the metal surface is shown in Figure 3c. We calculated it by shifting an adsorbate rigidly closer and farther from the slab with respect to the equilibrium position at the potential energy surface. Around the equilibrium distance, the work function depends almost linearly on the distance, and the slope is of 1.16 eVÅ^{-1} with the PBE functional and of 1.18 eV Å^{-1} with HSE06. The $\Delta\phi$ with HSE06 is about 0.06 eV larger than with the PBE functional. A change of adsorption distance as the one observed between the deuterated and normal cyclohexane (0.01 Å) would thus result in an isotope effect on $\Delta\phi$ of 16-17 meV, which does not strongly depend on the functional. In experiment,[2] the same qualitative trend was observed, but a slightly larger isotope effect on $\Delta\phi$ was reported, namely of ≈ 25 meV at $\theta = 0.46$. This value was obtained by a linear regression of the experimental data for the $\Delta\phi$ dependence on coverage reported in Ref. [2], in the interval $0.1 < \theta < 0.65$, followed by an alignment of the fits such that they yield $\Delta\phi = 0$ at θ=0. In Figure S5, Supporting Information, we show that larger coverages considerably increase the value and the slope of $\Delta\phi$ with distance from the surface, but the inclusion of self-consistent vdW interactions does not change appreciably the values or the slopes of $\Delta\phi$.

The origin of the work-function change upon the adsorption of a neutral and non-polar adsorbate like cyclohexane, is typically attributed i) to the so-called "pushback effect," when molecules "push" the vacuum tail of the electron density of the metal back into a surface,[22,23] and ii) to the polarization of the adsorbate induced by the mirror image charge formed in metal.[24] By analyzing electronic charge density differences from PBE, shown in **Figure 4**, we observe the pushback effect but also density rearrangements that are typical of weak bond formation. To visualize this, the electronic densities were integrated over the directions parallel to the surface and projected in the perpendicular direction (Figure 4a). The total electronic density of the interface was compared with the sum of the electronic densities of the clean surface and the isolated adsorbate. We observe an electron depletion in the C-H bonds and accumulation in the H…Rh region, which is associated with H-Rh bond formation. It is accompanied by the pushback effect similar to what was reported by Bagus et al. for cyclohexane on a Cu(111) cluster.[23] In Figure 4b, the redistribution of the electron density on a plane perpendicular to the surface, that crosses only carbon–carbon

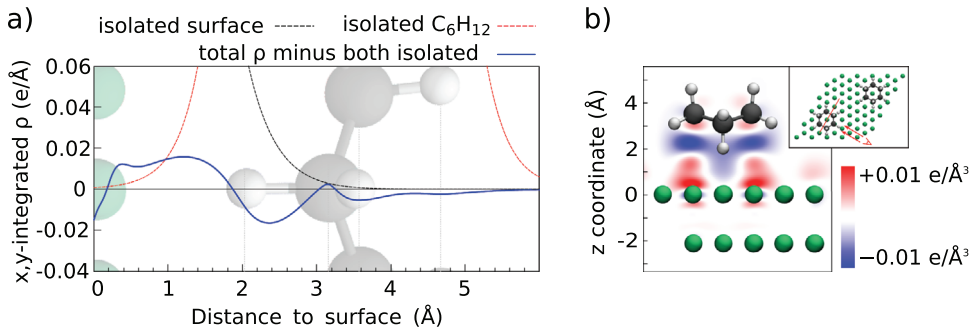

Figure 4. a) The electron density ρ of the interface integrated over the x and y dimensions and projected on the z axis (PBE functional). The dashed lines represent the electron densities of the clean surface and the adsorbate monolayer, calculated separately. The blue line shows difference between the total density and the superposition of isolated parts. It shows the density accumulation between Rh and H atoms and the depletion in C-H bond. b) The difference between the total electron density of the interface and the sum of the densities of the clean surface and the isolated adsorbate. Blue shows electron depletion, and red shows accumulation. The inset shows the unit cell and the slicing plane (the dashed red line). The position of the plane is chosen as shown in the inset.

bonds, is shown. In this plane, the contribution of H-metal bonds is small, therefore the electron depletion that is present under the molecule can be attributed to a pushback effect. It is difficult to separate the role of H-metal bond formation and the pushback effect. By investigating the spatial arrangement of the electronic density changes, we conclude that the contributions of these two effects are of comparable magnitudes (see Figures S6 and S7, Supporting Information). Together, H-metal bonds and a pushback effect cause a 2.13 Debye per molecule decrease in the dipole moment of the interface.

2.2. Validity of the Quasi-Harmonic Analysis

The quasi-harmonic treatment and the relationship between the distance of the molecule to the surface and the work function change already provide a qualitative explanation about the electronic structure changes that take place upon isotopic substitution. At this point, it is interesting to gauge the accuracy the quasi-harmonic approximation in these types of interfaces.

Path integral molecular dynamics (PIMD), a method which exploits the quantum-classical isomorphism between a quantum system and a classical ring polymer with infinite number of beads P,[9] can be employed in this context, in order to calculate static thermodynamic averages without relying on any harmonic ansatz. When performed on ab initio potentials (aiPIMD), subsequent analysis can capture the coupling between quantum molecular vibrations and the electronic structure of a surface in the adiabatic limit, with full anharmonicity and full dimensionality.

However, given the need of a first-principles potential energy surface and the large system sizes involved, aiPIMD simulations of this sort are associated with a high simulation cost, because of the need of several replicas of the full system to obtain converged results (the number of beads P, which controls the convergence of PIMD results to exact quantum expectation values). In order to alleviate this cost, one can use the fact that the bonding between molecules and a surface is relatively weak in the case of cyclohexane, to apply the spatially-localized ring-polymer contraction (SL-RPC).[10] The core idea of this contraction is sketched in Figure 6a. The potential energy (and the corresponding forces) of the full system of P beads is approximated as a superposition of P replicas of the molecular part, $P' \ll P$ replicas of the full system, and additional P' replicas of the molecular part with negative sign, that is,

$$V_P(\boldsymbol{q}) \approx \frac{P}{P'} \sum_{k=1}^{P'} \left[V_{\text{full}}(\tilde{\boldsymbol{q}}^{(k)}_{\text{full}}) - V_{\text{mol}}(\tilde{\boldsymbol{q}}^{(k)}_{\text{mol}}) \right] + \sum_{k=1}^{P} V_{\text{mol}}(\boldsymbol{q}^{(k)}_{\text{mol}}) \tag{1}$$

where "full" denotes the full system containing the surface and adsorbed molecules, and "mol" denotes the adsorbate simulated in the same unit cell, but without the surface. $\boldsymbol{q}^{(k)}$ are Cartesian positions of beads, and $\tilde{\boldsymbol{q}}^{(k)}$ are obtained by the Fourier interpolation of the full P beads ring polymer to the contracted P'-polymer.

This approximation, of course, does not come without errors. One can estimate the error introduced by SL-RPC in a harmonic potential[10]

$$\delta E^{\text{RPC}} = E^{\text{RPC}} - E^{\text{P beads}} = \sum_{i=1}^{3N} \frac{k_B T}{2} \sum_{k=P'}^{P-1} \left[\frac{\omega^2_{\text{mol}}}{\omega_k^2 + \omega^2_{i,\text{mol}}} - \frac{\omega^2_{\text{full}}}{\omega_k^2 + \omega^2_{i,\text{full}}} \right] \tag{2}$$

where $\{\omega_{i,\text{mol}}\}$ are normal mode frequencies of the isolated adsorbate, and $\{\omega_{i,\text{full}}\}$ are the corresponding frequencies calculated by diagonalization of the part of Hessian matrix that describes molecular displacements. Equation (2) is slightly different from Equation (9) in ref. [10] because we have not made the assumption of $\omega^2_{\nu,\text{mol}} - \omega^2_{\nu,\text{full}} \ll \omega_k^2 + \omega^2_{\nu,\text{full}}$, as discussed in Section S7, Supporting Information.

Similarly, one can estimate the error in a harmonic quantum free energy at finite temperatures (see the derivation in Section S8, Supporting Information) as,

$$\delta F^{RPC} = \frac{1}{2\beta} \sum_{i=1}^{3N} \sum_{k=P'}^{P-1} \ln\left(1 + \frac{\omega^2_{i,\text{full}} - \omega^2_{i,\text{mol}}}{\omega_k^2 + \omega^2_{i,\text{mol}}} \right) \tag{3}$$

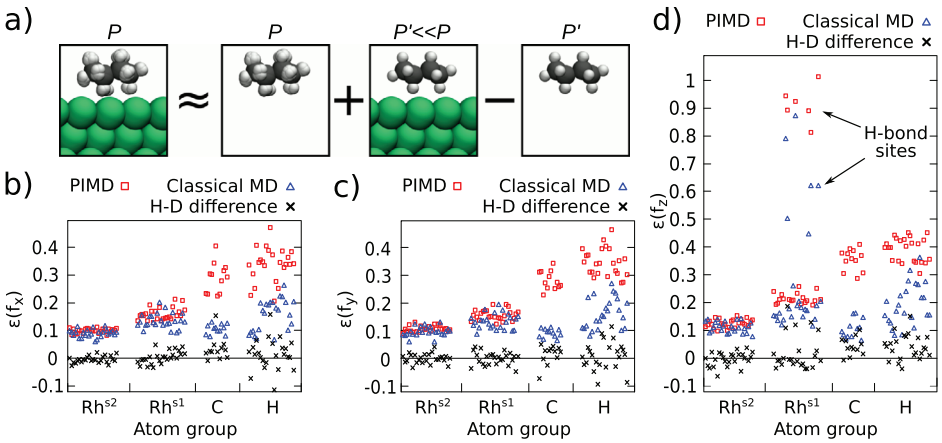

Figure 5. a) A scheme of the spatially-localized ring polymer contraction (SL-RPC). The forces for a full ring polymer of P beads are approximated by a superposition of forces calculated for P beads at the molecular part, $P' < P$ beads of the full system and a correction of P' beads at the molecular part. b,c) Anharmonicity measure ϵ (see Equation (4)) for individual Cartesian x and y components of atomic forces from the PIMD simulation of C_6H_{12} (red squares) compared to classical-nuclei MD (blue triangles), and difference in ϵ between PIMD simulations of C_6H_{12} and C_6D_{12} (black crosses). All values calculated for $\theta = 0.46$ (two cyclohexane molecules in the unit cell), with the PBE + vdW^{surf} functional, and at $T = 150$ K. Rh^{s1} and Rh^{s2} denote the 1st and the 2nd layers of the surface atoms. d) Anharmonicity measure ϵ for the Cartesian z component of the forces. The distinct group of Rh atoms with highly anharmonic forces consists of atoms connected to cyclohexane via hydrogen-metal bonds.

Such an estimate for cyclohexane on Rh(111), when taking $P' = 1$ does not exceed 37 meV per molecule for the total potential energy and 79 meV per molecule for the total free energy. When comparing H- and D-cyclohexane, one can rely on error cancellation. Then, the error in potential energy difference is 19 meV per molecule, and in free energy difference about 36 meV per molecule. It is thus clear that although this approximation is very useful, if quantitative results for this particular system are desired, a contraction to the centroid ($P' = 1$) is not sufficient and we do not further pursue calculations of free energies at this level of approximation. It should, however, be sufficient to capture further important anharmonic effects if present.

Before analyzing the PIMD results, we study the anharmonic contributions to the forces in this system, separating them into classical finite temperature effects and nuclear quantum effects. For this purpose, we follow the lines of ref. [25] and calculate an anharmonicity measure for different degrees of freedom. Because it is interesting to compare the difference between quantum and classical anharmonic contributions to different coordinates in the system, we calculate

$$\epsilon(T)^{\mathrm{CL/QM}} = \sqrt{\frac{\langle (F_{\mathrm{DFT}}^{\mathrm{CL/QM}} - F_{\mathrm{h}}^{\mathrm{CL/QM}})^2 \rangle_T}{\sigma^2_{F_{\mathrm{DFT}}^{\mathrm{QM}}}(T)}} \tag{4}$$

where F_{DFT} are the full DFT forces, F_{h} are harmonic forces calculated for the same geometry and with the Hessian matrix obtained for the full system at equilibrium, σ^2 is the variance, and $\langle \dots \rangle_T$ is the ensemble average at the temperature T. The superscripts CL and QM denote a classical-nuclei (aiMD) and a quantum-nuclei (aiPIMD) simulations, respectively. In the latter case, we take the forces on the bead positions. We normalize both classical and quantum quantities by the respective aiPIMD variance of that quantity so that the difference $\epsilon(T)^{\mathrm{QM}} - \epsilon(T)^{\mathrm{CL}}$ corresponds to a measure of the amount of "quantum anharmonicity."

We show the results of this analysis for C_6H_{12} and C_6D_{12} in **Figure 5** (b–d), where the force components are resolved into the three Cartesian directions (all calculations with PBE+vdW^{surf}). Such an analysis shows, as expected, that anharmonic contributions are more pronounced in the adsorbate molecules, and the difference between quantum and classical anharmonic scores is really only pronounced on the molecular adsorbate. However, bonding sites on the top layer of the surface show not only a pronounced anharmonicity in the z direction, but also a considerable quantum component, no doubt caused by the nuclear quantum contributions to the H-metal bond. In fact, comparing the z component of the forces with the x and y components, the z anharmonic score is always higher for the top surface layer and the molecules. This supports the conclusion that most anharmonic effects lie on the out-of-plane motions of molecules, which are captured to a limited extent in the QH approximation. However, these calculations also show that the contribution of quantum anharmonicity on C_6H_{12} and C_6D_{12} is similar, suggesting that they could play a minor role for the evaluation of isotope effects in this potential energy surface.

2.3. Analysis of PIMD Results

From the aiMD and aiPIMD simulations (PBE+vdW^{surf}), we could directly estimate structural properties of the classical and quantum C_6H_{12} and C_6D_{12} on Rh(111) at 150 K. In addition, we could capture changes in the electronic structure including full electron-phonon coupling at the adiabatic limit, by averaging the desired electronic quantities of interest over the trajectories. The only drawback, as we will see below, is that even with the SL-RPC technique, statistically converging the quite small energy differences and structural changes observed upon deuteration is a very challenging task. Each force evaluation containing the full interface with the model $\theta = 0.46$ (FHI-aims program, *light* settings) amounts, on average, to 3.1 min when parallelized over

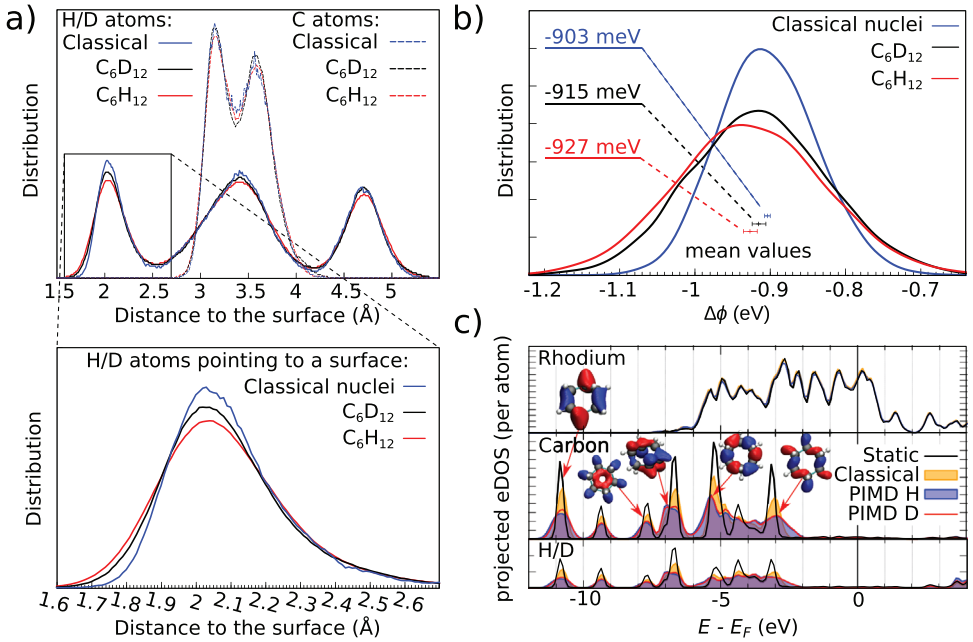

Figure 6. a) The distribution of distances from the Rh(111) surface to H/D atoms (solid lines) and C atoms (dashed lines). The red (black) lines show PIMD simulations of C_6H_{12} (C_6D_{12}), and the blue lines represent MD simulations with classical nuclei. b) The distribution of $\Delta\phi$ values for PIMD simulations of C_6H_{12} (red), C_6D_{12} (black), and classical MD simulation (blue). c) The species-projected electronic density of states in a single-point calculation (black), a classical-nuclei MD simulation (yellow), and PIMD simulations for C_6H_{12} (blue) and C_6D_{12} (red). Peaks are broadened and shifted due to coupling with nuclear vibrations. Typical Kohn–Sham eigenstates are shown near the corresponding peaks. In all panels, $T = 150$ K.

240 cores (Intel Xeon Gold 6148 Skylake processors, COBRA supercomputer). This cost renders these simulations computationally expensive even without considering nuclear quantum effects. Even so, we ensured at least 30 ps of trajectories for each of the systems that we consider (see Experimental Section).

The results are summarized in **Figure 6**a–c. In panel a, we show the distribution of the distance from the adsorbate atoms to the top layer of the Rh(111) surface. As expected, a more localized position distribution is observed for C_6D_{12} than for C_6H_{12}, and it is even more localized for classical-nuclei cyclohexane. The inset in panel a shows that C_6H_{12} can reach closer to the surface than C_6D_{12} and classical-nuclei cyclohexane, but it was not possible to resolve differences on the average position h_{COM} to an accuracy of 0.01 Å.

In Figure 6b, the distribution of work function values at 150 K is shown. Again, C_6H_{12} presents a broader distribution than C_6D_{12} and classical-nuclei MD. The distributions are shifted with respect to each other, and their mean values $\langle\Delta\phi\rangle$ are ordered so that $\langle\Delta\phi\rangle_H < \langle\Delta\phi\rangle_D < \langle\Delta\phi\rangle_{Classical}$. The resulting values for $\langle\Delta\phi\rangle$ are –927 ± 9 meV for C_6H_{12}, –915 ± 9 meV for C_6D_{12}, and –903 ± 5 meV for classical-nuclei cyclohexane. We were careful in evaluating these uncertainties, by analyzing the autocorrelation behavior of this quantity during the simulation. The H/Classical difference is 24 ± 10 meV and we expect the H/D difference to be between zero and this value. In fact, we compute the H/D difference to be 12 ± 13 meV, which, despite the large uncertainty, shows the expected trend. Compared to the QH approximation, the aiMD and aiPIMD simulations predict the molecules (with either classical or quantum nuclei) to lie farther away from the surface ($h_{COM} = 3.42 \pm 0.01$ Å) by around 0.06 ± 0.01 Å (See estimation of h_{COM} within the QH approximation including temperature effects in Section S4, Supporting Information). Accordingly, the aiPIMD simulations predict a considerably smaller overall work function change. This is a consequence of taking into account anharmonic contributions at a temperature of 150 K (we note that the rigid "out of plane" vibrations of the adsorbates lie around 80–130 cm^{-1}, thus having components that are thermally activated at 150 K). This is also consistent with the high anharmonic score of the forces in the z direction, especially at bonding sites. Statistically converging the differences between C_6H_{12} and C_6D_{12} would require a considerable computational effort. However, with the current uncertainty intervals, it is possible to conclude that the isotope effects from the aiPIMD simulations cannot differ largely from the QH results, confirming that anharmonic contributions play a minor role on the geometric isotope effects in this potential energy surface. We were not able to calculate the isotope effect on the binding energies because, as mentioned previously, the SL-RPC approximation would have to include (many) more replicas of the system for an accurate assessment, which would make the calculations prohibitive.

The aiPIMD simulations, nevertheless, give access to the electron density of states renormalized by the quantum fluctuations of the molecules. We project the total electronic density of states on the atomic species and average it over multiple snapshots of the simulations. The results are compared with the static density of states in Figure 6c. There is a pronounced broadening of the peaks only on the adsorbate (for both quantum and classical nuclei), and this broadening is much more pronounced when considering quantum nuclei. We note that it is not clear if one can assign any physical interpretation to such broadening of Kohn–Sham single-particle orbitals. Nevertheless, this effect is caused by the dependence of these ground-state orbital energies

on nuclear configurations and the interplay of this dependence with the distribution of nuclear configurations. In addition, there are considerable energy shifts due to this electron-phonon interaction in levels associated with sp^3 orbitals. Since sp^3 orbitals are responsible for C-H bonding, we tentatively correlate these shifts with the interplay of ZPE and anharmonicity, which effectively changes bond-lengths and thus the electronic structure in this system. The semilocal/nonlocal functionals we employ are not able to provide a quantitative level alignment of this interface, even if they can predict the HOMO level reasonably well because of the cancellation of the self-interaction error and the missing image-potential effect.[26,27] Even though a much higher level of theory (e.g., many-body perturbation theory) would be desirable for a quantitative comparison with UPS experiments conducted at this interface,[15] the magnitude of changes that we observe in the Kohn–Sham electronic density of states highlights the importance of taking nuclear fluctuations into account when analysing the electronic spectra of such interfaces.

3. Conclusions

In summary, we have studied isotope and anharmonic effects on the cyclohexane/Rh(111) interface by means of DFT calculations coupled to harmonic lattice dynamics, aiMD, and aiPIMD.

Employing a QH approximation, in which the harmonic ZPE contributions were calculated with the molecule fixed at different distances from the surface, it could be shown that the binding energy of C_6D_{12} is smaller than that of C_6H_{12} and that C_6D_{12} lies 0.01 Å farther from the surface than C_6H_{12}, in qualitative agreement with the isotope effects previously observed experimentally[2] at the same interface. By showing that the work-function change of the interface is very sensitive to the molecule-surface distance, this geometrical isotope effect could be correlated with the isotope-induced change in the work function, thus confirming the hypothesis that Koitaya, Yoshinobu, and coworkers proposed,[3] based on experimental observations. Finally, these simulations also showed that the electronic-density rearrangement at the interface is impacted by both bond formation and the pushback effect and that the inclusion of van der Waals contributions, improve the energetics and adsorption distances.

The reliability of the QH approximation was assessed by estimating the degree of anharmonicity of the nuclear motions at a temperature of 150 K. Anharmonic contributions to the forces are particularly pronounced at surface sites that bond to hydrogens and on the degrees of freedom belonging to the adsorbates. In these cases, in particular, the difference between classical and quantum anharmonic contributions is also large, meaning that techniques like PIMD are necessary to describe structural aspects and related electron-phonon interactions in these systems. However, the quantum part of the anharmonic contributions to C_6H_{12} and C_6D_{12} are very similar in magnitude and character for coordinates parallel to the surface, and thus play a minor role when addressing isotope effects. This explains why the QH approximation fares well for these quantities in this case.

Indeed, in the aiMD and aiPIMD simulations, the pronounced anharmonic character of certain degrees of freedom in the direction perpendicular to the surface plane cause the equilibrium distance of the adsorbates to be around 0.06 Å farther from the surface than a static evaluation or the QH approximation would predict. This effect stems mostly from anharmonic terms that are already captured with classical nuclei. This is accompanied by considerably smaller work function changes. However, as expected due to the small contribution of quantum anharmonic effects beyond the QH approximation and within the statistical error bars, the observed isotope effects on this system (distance to surface and work function change) do not differ significantly from the QH case. Finally, the effect of electron-phonon coupling on the electronic density of states in the adiabatic limit causes a pronounced shift (and broadening) of Kohn–Sham levels related to the CH bonds.

Although we obtain excellent qualitative agreement with experiment and are able to provide an atomistic view on the origins of the isotope effects measured in this interface, there are still remaining differences in the magnitude of the isotope effect, in particular on the adsorption energy. We are left with the conclusion that this disagreement is likely coming from slightly different conditions in experiment caused by, for example, clustering of molecules at lower coverages, or the remaining approximations that were employed in this work. The most prominent approximations are the DFT functional and the SL-RPC approximation. We also cannot rule out that very slow degrees of freedom are not sufficiently sampled within the dynamical simulations. Nevertheless, we suggest that the exchange-correlation functional would be the largest source of remaining errors, given the known drawbacks that functionals based on generalized gradient approximations present for adsorbates on metallic surfaces,[28] and the scatter of binding energies and distances we observed for different functionals and vdW corrections. Moreover, the functionals that yield good binding energies in comparison to experiment, seem to predict a work-function variation with distance to the surface that is too small. All of these observations motivate the training of fitted or machine-learned potentials that include long-range electrostatic interactions[29] and are based on more accurate potential energy surfaces.[30,31] Such potentials would both decrease the cost related to statistical sampling and increase the (quantitative) predictive power of these simulations.

4. Experimental Section

Electronic Structure Calculations with FHI-Aims: Energies and forces are calculated using DFT with the PBE exchange-correlation (XC) functional[32] and the range-separated hybrid HSE06 functional.[20] The calculations were done with the all-electron FHI-aims code, which uses numerical atom-centered orbitals[33] as basis sets. The FHI-aims package contains predetermined settings for numerical parameters and basis sets, which are aimed at different accuracy levels. *Light* settings were used for PIMD and phonon calculations, and *tight* settings were used for potential energy curves and electron density rearrangement. The parameters of Rh for the pairwise Tkatchenko–Scheffler van der Waals correction modified in order to capture the collective response of a surface in the Lifshitz–Zaremba–Kohn form[18] (vdW^{surf}) were taken from ref. [34]. The van der Waals interaction between Rh atoms was not included. Further, $\beta = 0.81$ was used for the nl-MBD correction with the PBE functional and $\beta = 0.83$ for the same correction with the HSE06 functional.

Four Rh(111) layers were considered in all FHI-aims calculations. The two bottom layers of the slab were fixed in the bulk geometry. The bulk geometry was calculated for the single-atom FCC unit cell using a 16x16x16 k-point grid. The k-point grid for the different surface unit cells were scaled accordingly. For the 5×5 Rh(111) surface unit cell, a $2 \times 2 \times 1$ k-point grid was employed. The resulting lattice constant of 3.83 Å was

in good agreement with the experimental value of 3.80 Å.[35] The surface was aligned perpendicular to the *z* axis. In order to isolate the system from its periodic replicas in the *z* direction, a dipole correction[36] and vacuum layer of 60 Å in was applied.

Vibrational analysis was performed by a modified version of the Phonopy code coupled to FHI-aims,[37,38] which allowed to build the Hessian only for the molecular adsorbate and to account for a surface as a rigid environment. This approximation is well justified because the coupling between Rh atoms and the molecules is weak, and this weak coupling is concentrated in the low-frequency modes of the adsorbates, which behave very similarly for H- and D-cyclohexane and thus do not impact isotope effects. Atomic displacements were set to 0.01 Å for finite difference calculations and geometries were relaxed with a maximum force threshold of 0.001 eV Å^{-1}.

Electronic Structure Calculations with Quantum Espresso: Calculations were carried out with the rev-vdW-DF2 XC functional,[21,39] a variant of the van der Waals density functional[40,41] as implemented in the Quantum ESPRESSO (QE)[42,43] plane-wave code. QE was used to calculate the adsorption energy and geometry of cyclohexane in a Rh(111) (5×5) surface unit cell ($\theta = 0.46$). The Rh(111) (5×5) surface was modeled by a 4 atomic layer slab with a vacuum equivalent to 17 monolayers (≈ 40 Å). The slab was constructed using the lattice constant optimized with rev-vdW-DF2 of 3.80 Å. The molecule was put on one side of the slab and the effective screening medium method was used to eliminate the artificial electrostatic interaction with the neighboring slabs.[44,45] The molecular geometry was optimized starting from that determined by FHI-aims. The bottom two layers of the slab were fixed and the remaining degrees of freedom were optimized until the force acting on them were less than 5×10^{-4} Ry/Bohr (1.3×10^{-2}eV Å^{-1}). Projector augmented wave[46] potentials from the pslibrary version 1.0.0[47] and a plane-wave basis set with a cutoff energy of 80 (640) Ry were used for wave functions (augmentation charge density). A 2×2 k-point grid was used to sample the surface Brillouin zone.

Adsorption Energies and Free Energies: The adsorption energies per molecule were calculated with

$$E_{\text{ads}}^{\text{pot}} = -(E_{\text{s+m}}^{\text{pot}} - E_{\text{s}}^{\text{pot}})/N_{\text{mol}} + E_{\text{m}}^{\text{pot}} \tag{5}$$

where $E_{\text{s+m}}^{\text{pot}}$ is the total energy at the potential energy surface of a slab with molecules adsorbed, $E_{\text{s}}^{\text{pot}}$ is the total energy of a clean surface relaxed with 2 bottom layers fixed in bulk position, $E_{\text{m}}^{\text{pot}}$ is the total energy of a molecule relaxed in vacuum, and N_{mol} is the number of molecules in a unit cell. A similar expression can be written for a free energy of adsorption $F_{\text{ads}}^{\text{harm}}$.

The harmonic vibrational free energy was calculated as

$$F^{\text{harm}} = \sum_{i=1}^{N_{\text{modes}}} \left[\frac{\hbar\omega_i}{2} + k_B T \ln\left(1 - \exp^{-\frac{\hbar\omega_i}{k_B T}}\right)\right] + {}_{\text{[if gas phase]}}\left(F^{\text{trans}} + F^{\text{rot}}\right) \tag{6}$$

where $N_{\text{modes}} = 3N - 3$ when the free energy of a clean surface is calculated (N is the number of atoms in a unit cell), $N_{\text{modes}} = 3N - 3N_s$ (N_s is the number of surface atoms in a unit cell) when the free energy of molecules adsorbed on surface is calculated, and $3N_m - 6$ (N_m is the number of atoms in a molecule), when the free energy of an isolated molecule is calculated. Rotational and translational contributions were added for the free molecule according to the rigid-body and ideal gas textbook expressions.[48] The expression above only takes into account vibrations at the Γ point of the unit cell. Because the focus was mostly on molecular vibrations, which showed a very small phonon band dispersion, and employed large surface unit cells, this approximation did not introduce large errors in the calculated free energy differences. For the translational term, a pressure of 10^{-8} Pa was taken, which is close to the reported experimental conditions.[2]

The quasi-harmonic ZPE-corrected energy of adsorption E_{ads}^{*} was calculated as a difference between the energy at the equilibrium distance and at 10 Å away from the surface, which is considered to be far enough to remove all molecule-surface interaction,

$$E_{\text{ads}}^{*}(h_{\text{COM}}) = \left(E_{\text{s+m}}^{\text{pot}}(h_{\text{COM}}) + \sum_{i=1}^{3N_m-3} \frac{\hbar\omega_i}{2}(h_{\text{COM}})\right) - \left(E_{\text{s+m}}^{\text{pot}} + \sum_{i=1}^{3N_m-3} \frac{\hbar\omega_i}{2}\right)\Bigg|_{h_{\text{COM}}=10\text{Å}} \tag{7}$$

where h_{COM} denotes the distance from the center of mass of the adsorbate to the Rh surface. Although E_{ads}^{*} is not a true adsorption energy, this procedure compensates spurious interactions that might appear in a particular simulation cell. For the ZPE contribution, $(3N_m - 3)$ molecular vibrations were included.

Ab Initio Molecular Dynamics: AiMD and aiPIMD simulations were carried out by connecting FHI-aims to the i-PI code.[49] For classical-nuclei MD, a timestep of 1 fs was used. For PIMD simulations, a smaller timestep of 0.5 fs was employed.

In order to accelerate sampling in the NVT ensemble, a colored-noise generalized Langevin thermostat (GLE)[50,51] was applied to the classical-nuclei aiMD simulations. For the aiPIMD simulations, the PIGLET thermostat was used.[52] This approach preserved quantum distribution and gave a fast convergence of observables with respect to the number of replicas. The parameters for the thermostats are: 8 fictitious degrees of freedom s,[51] and a frequency range of 0.32–3200 cm^{-1} for C_6H_{12} and 0.23–2300 cm^{-1} for C_6D_{12}. The A and C matrices (as defined in ref. [51]) were parameterized for $\hbar\omega/k_BT = 50$ using the GLE4MD library.[53] Convergence with around 12 beads for the adsorbate atoms (H) at 150 K within this setup was observed. After thermalization, 7 independent trajectories of total length of 32 ps for C_6H_{12}, 5 trajectories of total length of 30 ps for C_6D_{12}, and 5 trajectories of total length of 97 ps for classical-nuclei cyclohexane were calculated.

The effects of nuclear fluctuations on electronic observables (work function, electronic density of states, etc.) were calculated as the average of single-point calculations from aiPIMD trajectories through the following general expression:

$$\langle A \rangle = \frac{1}{Z}\text{Tr}\left[\hat{A}e^{\frac{-\hat{H}}{k_BT}}\right] \xrightarrow[\text{PIMD sampling}]{\text{ergodicity,}} \frac{1}{PN_s}\sum_{i}^{N_s}\sum_{k}^{P} A\left(\boldsymbol{q}^{(k)}(t_i)\right) \tag{8}$$

where $\hat{A}$ is a position-dependent observable, $\hat{H}$ is the Hamiltonian, Z is the partition function, P is the number of beads of a ring polymer, N_s is the number of snapshots considered from a PIMD trajectory, and $\boldsymbol{q}^{(k)}$ is a position vector for a bead k. The snapshots from the PIMD trajectory were picked so that they were statistically independent. The criterion for independence was an autocorrelation time of the property A. In the PIMD calculations, the autocorrelation time was 30 fs for a velocity, 300 fs for a work function, and 600 fs for the z-coordinate of the center of mass of a molecule. These correlation times were also used to calculate error bars. For classical nuclei simulations, the same expression was used with $P = 1$.

Supporting Information

Supporting Information is available from the Wiley Online Library or from the author.

Acknowledgements

The authors acknowledge fruitful and enlightening discussions with Prof. Jun Yoshinobu and Prof. Takanori Koitaya, who have also motivated this work with their experiments and initial hypothesis. M.R. and K.F. acknowledge financial support from the International Max Planck Research School on Functionalized Interfaces (Max Planck Society). I.H. acknowledges financial support from Japan Society for the Promotion of Science through

Grant-in-Aid for Scientific Research on Innovative Areas "Hydrogenomics" (Grant No. JP18H05519). M.R. and K.F. further acknowledge lively scientific discussions about this work with Dmitrii Maksimov and Yair Litman. I.H. acknowledges discussions with Prof. Toshiki Sugimoto. Most of the computational time was provided by the Max Planck Computing and Data Facility (MPCDF), and part of the computation was performed at Research Institute for Information Technology, Kyushu University.

Open access funding enabled and organized by Projekt DEAL.

Correction added on 18 January 2021, after first online publication: Projekt Deal funding statement has been added.

Conflict of Interest

The authors declare no conflict of interest.

Keywords

density functional theory, isotope effect, path integral molecular dynamics, weakly bonded interfaces

Received: September 30, 2020
Revised: December 22, 2020
Published online:

[1] F. Giustino, *Rev. Mod. Phys.* **2017**, *89*, 015003.
[2] T. Koitaya, S. Shimizu, K. Mukai, S. Yoshimoto, J. Yoshinobu, *J. Chem. Phys.* **2012**, *136*, 214705.
[3] T. Koitaya, J. Yoshinobu, *Chem. Rec.* **2014**, *14*, 848.
[4] Y. Morikawa, H. Ishii, K. Seki, *Phys. Rev. B* **2004**, *69*, 041403.
[5] L. Li, X. Mu, W. Liu, Z. Mi, C.-J. Li, *J. Am. Chem. Soc.* **2015**, *137*, 7576.
[6] N. Koch, *ChemPhysChem* **2007**, *8*, 1438.
[7] M. Jacobs, J. Krumland, A. M. Valencia, H. Wang, M. Rossi, C. Cocchi, *Adv. Phys.: X* **2020**, *5*, 1749883.
[8] C. E. Patrick, F. Giustino, *J. Phys.: Condens. Matter* **2014**, *26*, 365503.
[9] M. Parrinello, A. Rahman, *J. Chem. Phys.* **1984**, *80*, 860.
[10] Y. Litman, D. Donadio, M. Ceriotti, M. Rossi, *J. Chem. Phys.* **2018**, *148*, 102320.
[11] A. Kaczmarek, M. Shiga, D. Marx, *J. Phys. Chem. A* **2009**, *113*, 1985, PMID: 19199678.
[12] W. Chen, F. Ambrosio, G. Miceli, A. Pasquarello, *Phys. Rev. Lett.* **2016**, *117*, 186401.
[13] Y. K. Law, A. A. Hassanali, *The Journal of Physical Chemistry A* **2015**, *119*, 10816, PMID: 26444383.
[14] T. Koitaya, K. Mukai, S. Yoshimoto, J. Yoshinobu, *J. Chem. Phys.* **2011**, *135*, 234704.
[15] T. Koitaya, K. Mukai, S. Yoshimoto, J. Yoshinobu, *J. Chem. Phys.* **2013**, *138*, 044702.
[16] K.-P. Bohnen, A. Eichler, J. Hafner, *Surf. Sci.* **1996**, *368*, 222.
[17] A. Tkatchenko, M. Scheffer, *Phys. Rev. Lett.* **2009**, *102*, 073005.
[18] V. G. Ruiz, W. Liu, E. Zojer, M. Scheffer, A. Tkatchenko, *Phys. Rev. Lett.* **2012**, *108*, 146103.
[19] J. Hermann, A. Tkatchenko, *Phys. Rev. Lett.* **2020**, *124*, 146401.
[20] A. V. Krukau, O. A. Vydrov, A. F. Izmaylov, G. E. Scuseria, *J. Chem. Phys.* **2006**, *125*, 224106.
[21] I. Hamada, *Phys. Rev. B* **2014**, *89*, 121103.
[22] H. Ishii, K. Sugiyama, E. Ito, K. Seki, *Adv. Mater.* **1999**, *11*, 605.
[23] P. S. Bagus, K. Hermann, C. Wöll, *J. Chem. Phys.* **2005**, *123*, 184109.
[24] K. Wandelt, J. E. Hulse, *J. Chem. Phys.* **1984**, *80*, 1340.
[25] F. Knoop, T. A. R. Purcell, M. Scheffer, C. Carbogno, *Phys. Rev. Mater.* **2020**, *4*, 083809.
[26] J. B. Neaton, M. S. Hybertsen, S. G. Louie, *Phys. Rev. Lett.* **2006**, *97*, 216405.
[27] J. M. Garcia-Lastra, C. Rostgaard, A. Rubio, K. S. Thygesen, *Phys. Rev. B* **2009**, *80*, 245427.
[28] R. J. Maurer, V. G. Ruiz, J. Camarillo-Cisneros, W. Liu, N. Ferri, K. Reuter, A. Tkatchenko, *Prog. Surf. Sci.* **2016**, *91*, 72.
[29] A. Grisafi, M. Ceriotti, *J. Chem. Phys.* **2019**, *151*, 204105.
[30] Z.-F. Liu, D. A. Egger, S. Refaely-Abramson, L. Kronik, J. B. Neaton, *J. Chem. Phys.* **2017**, *146*, 092326.
[31] O. T. Hofmann, V. Atalla, N. Moll, P. Rinke, M. Scheffer, *New J. Phys.* **2013**, *15*, 123028.
[32] J. P. Perdew, K. Burke, M. Ernzerhof, *Phys. Rev. Lett.* **1996**, *77*, 3865.
[33] V. Blum, R. Gehrke, F. Hanke, P. Havu, V. Havu, X. Ren, K. Reuter, M. Scheffer, *Comput. Phys. Commun.* **2009**, *180*, 2175.
[34] V. G. Ruiz, W. Liu, A. Tkatchenko, *Phys. Rev. B* **2016**, *93*, 035118.
[35] J. W. Arblaster, *Platinum Metals Review* **1997**, *41*, 184.
[36] J. Neugebauer, M. Scheffer, *Phys. Rev. B* **1992**, *46*, 16067.
[37] A. Togo, I. Tanaka, *Scr. Mater.* **2015**, *108*, 1.
[38] Modified Phonopy-FHI-aims interface, https://github.com/fidanyan/phonopy (accessed: September 2019).
[39] M. Callsen, I. Hamada, *Phys. Rev. B* **2015**, *91*, 195103.
[40] T. Thonhauser, V. R. Cooper, S. Li, A. Puzder, P. Hyldgaard, D. C. Langreth, *Phys. Rev. B* **2007**, *76*, 125112.
[41] K. Berland, V. R. Cooper, K. Lee, E. Schröder, T. Thonhauser, P. Hyldgaard, B. I. Lundqvist, *Rep. Prog. Phys.* **2015**, *78*, 066501.
[42] P. Giannozzi, S. Baroni, N. Bonini, M. Calandra, R. Car, C. Cavazzoni, D. Ceresoli, G. L. Chiarotti, M. Cococcioni, I. Dabo, A. Dal Corso, S. de Gironcoli, S. Fabris, G. Fratesi, R. Gebauer, U. Gerstmann, C. Gougoussis, A. Kokalj, M. Lazzeri, L. Martin-Samos, N. Marzari, F. Mauri, R. Mazzarello, S. Paolini, A. Pasquarello, L. Paulatto, C. Sbraccia, S. Scandolo, G. Sclauzero, A. P. Seitsonen, et al., *J. Phys.: Condens. Matter* **2009**, *21*, 395502.
[43] P. Giannozzi, O. Andreussi, T. Brumme, O. Bunau, M. B. Nardelli, M. Calandra, R. Car, C. Cavazzoni, D. Ceresoli, M. Cococcioni, N. Colonna, I. Carnimeo, A. Dal Corso, S. de Gironcoli, P. Delugas, R. A. DiStasio, A. Ferretti, A. Floris, G. Fratesi, G. Fugallo, R. Gebauer, U. Gerstmann, F. Giustino, T. Gorni, J. Jia, M. Kawamura, H.-Y. Ko, A. Kokalj, E. Küçükbenli, M. Lazzeri, et al., *J. Phys.: Condens. Matter* **2017**, *29*, 465901.
[44] M. Otani, O. Sugino, *Phys. Rev. B* **2006**, *73*, 115407.
[45] I. Hamada, M. Otani, O. Sugino, Y. Morikawa, *Phys. Rev. B* **2009**, *80*, 165411.
[46] P. E. Blöchl, *Phys. Rev. B* **1994**, *50*, 17953.
[47] A. Dal Corso, *Comput. Mater. Sci.* **2014**, *95*, 337.
[48] L. D. Landau, E. M. Lifshitz, *Statistical Physics*, Part 1, Vol. *5*, 3rd ed., Butterworth-Heinemann, Oxford **1980**.
[49] V. Kapil, M. Rossi, O. Marsalek, R. Petraglia, Y. Litman, T. Spura, B. Cheng, A. Cuzzocrea, R. H. Meißner, D. M. Wilkins, B. A. Helfrecht, P. Juda, S. P. Bienvenue, W. Fang, J. Kessler, I. Poltavsky, S. Vandenbrande, J. Wieme, C. Corminboeuf, T. D. Kühne, D. E. Manolopoulos, T. E. Markland, J. O. Richardson, A. Tkatchenko, G. A. Tribello, V. V. Speybroeck, M. Ceriotti, *Comput. Phys. Commun.* **2019**, *236*, 214.
[50] M. Ceriotti, G. Bussi, M. Parrinello, *Phys. Rev. Lett.* **2009**, *102*, 020601.
[51] M. Ceriotti, G. Bussi, M. Parrinello, *J. Chem. Theory Comput.* **2010**, *6*, 1170.
[52] M. Ceriotti, D. E. Manolopoulos, *Phys. Rev. Lett.* **2012**, *109*, 100604.
[53] Laboratory of Computational Science and Modelling, EPFL Lausanne, Switzerland, GLE4MD, http://gle4md.org (accessed: August 2020).